Electronic Supplementary Material (ESI) for Physical Chemistry Chemical Physics.

Supplementary Information

Molecular Insights into the Oligomerization Dynamics and Conformations of Amyloidogenic and Non-Amyloidogenic Amylin from Discrete Molecular Dynamics Simulations

Ying Wang[1], Yuying Liu[1], Yu Zhang[1], Guanghong Wei[2], Feng Ding[3], Yunxiang Sun[1,2,3]*

[1]Department of Physics, Ningbo University, Ningbo 315211, China

[2]State Key Laboratory of Surface Physics and Department of Physics, Fudan University, Shanghai 200433, P. R. China

[3]Department of Physics and Astronomy, Clemson University, Clemson, SC 29634, USA.

*E-mail: sunyunxiang@nbu.edu.cn;

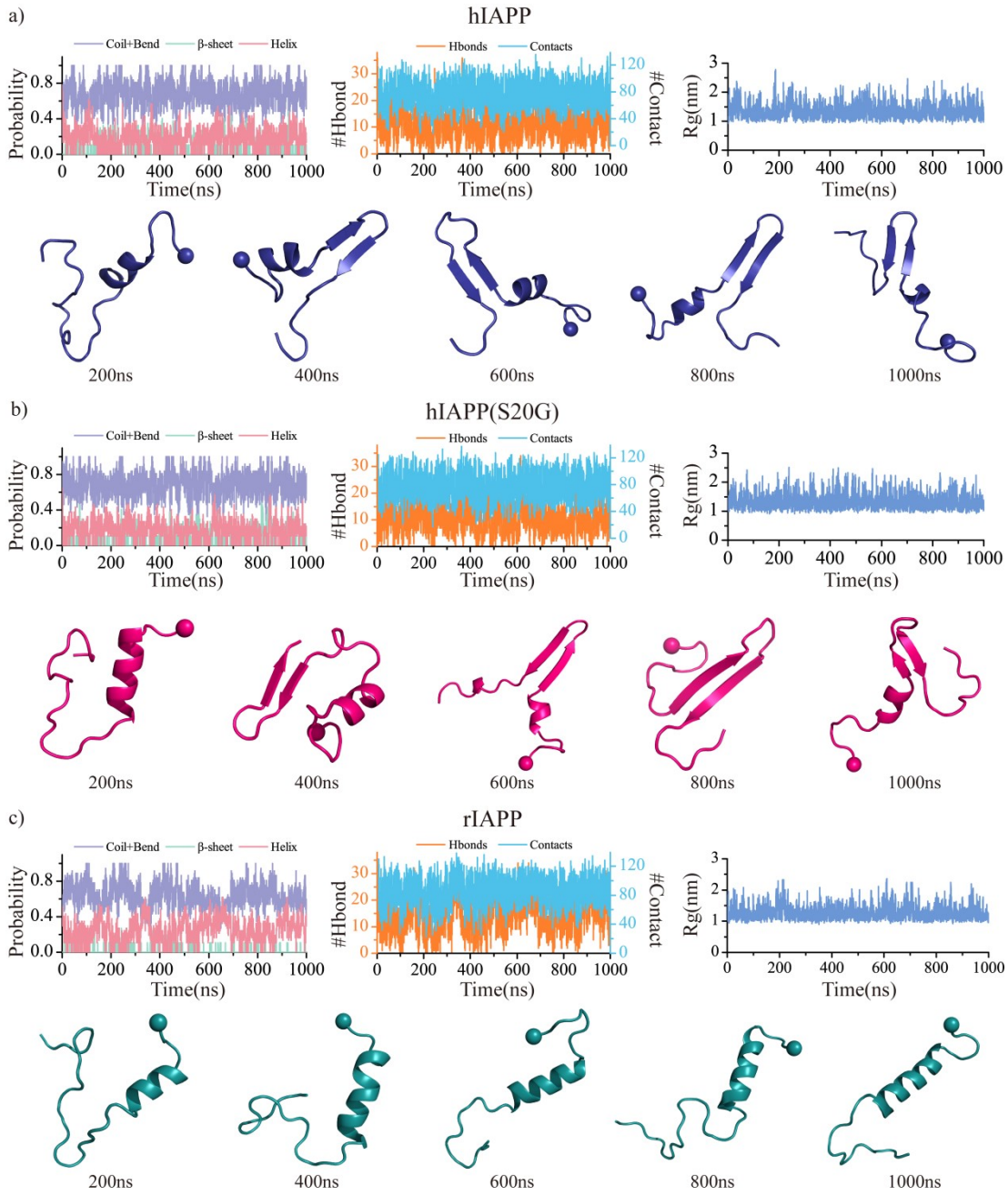

Fig. S1. Time evolution of the probability of unstructured formations (bend and random coil), helix and β-sheet, the number of hydrogen bonds and contact, and the radius gyration for the monomeric hIAPP a), hIAPP(S20G) b), and rIAPP c) peptide. One trajectory was randomly selected from 60 independent DMD simulation trajectories for each monomeric system. The N-terminal Cα atom is highlighted as a bead.

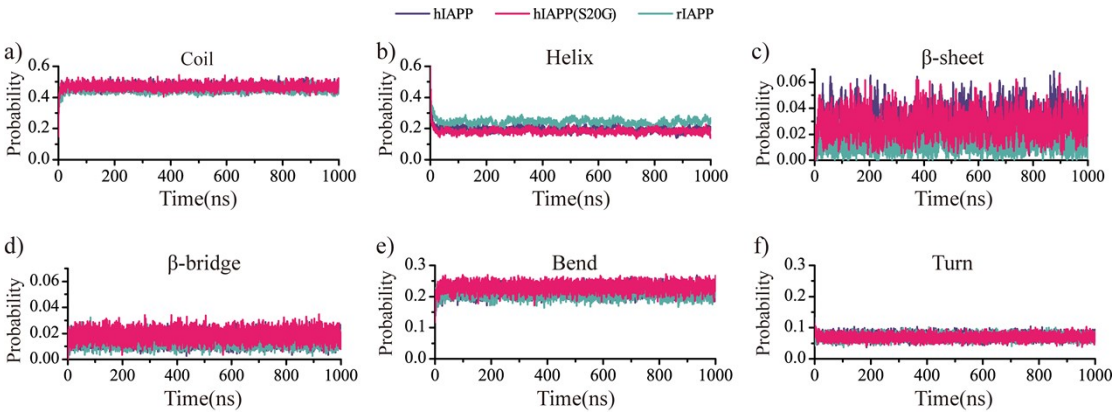

Fig. S2. Time evolution of averaged probability of each secondary structure (including coil, helix, β-sheet, β-bridge, bend, and turn) for the monomeric hIAPP, hIAPP(S20G), and rIAPP peptide using 60 independent DMD simulation trajectories.

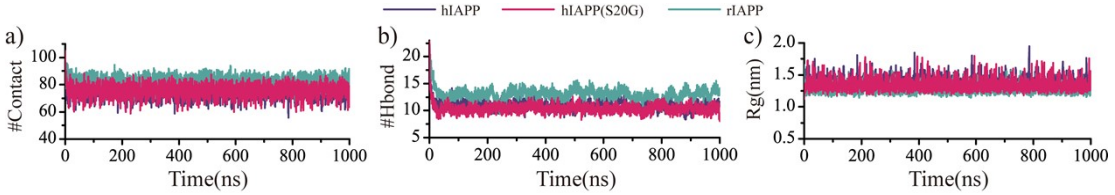

Fig. S3. Time evolution of the number of contacts, hydrogen bonds, and radius gyration (Rg) of the monomeric hIAPP, hIAPP(S20G), and rIAPP peptide averaged over the 60 independent DMD simulations.

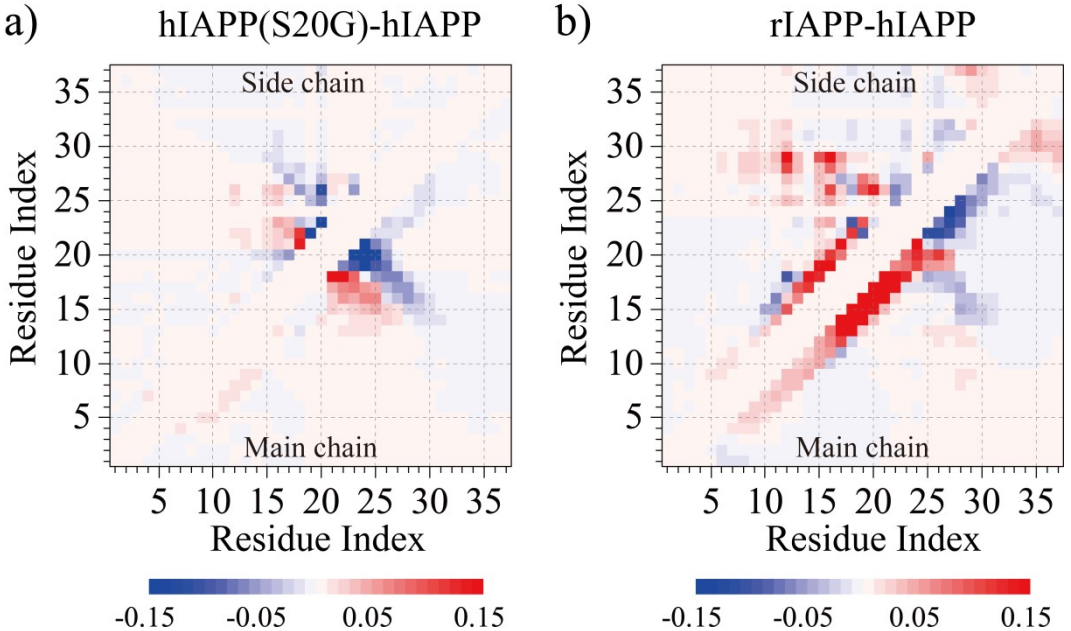

Fig. S4. The difference of residue pairwise contact frequency for the monomers of hIAPP(S20G) a) and rIAPP b) compared with the wild type hIAPP.

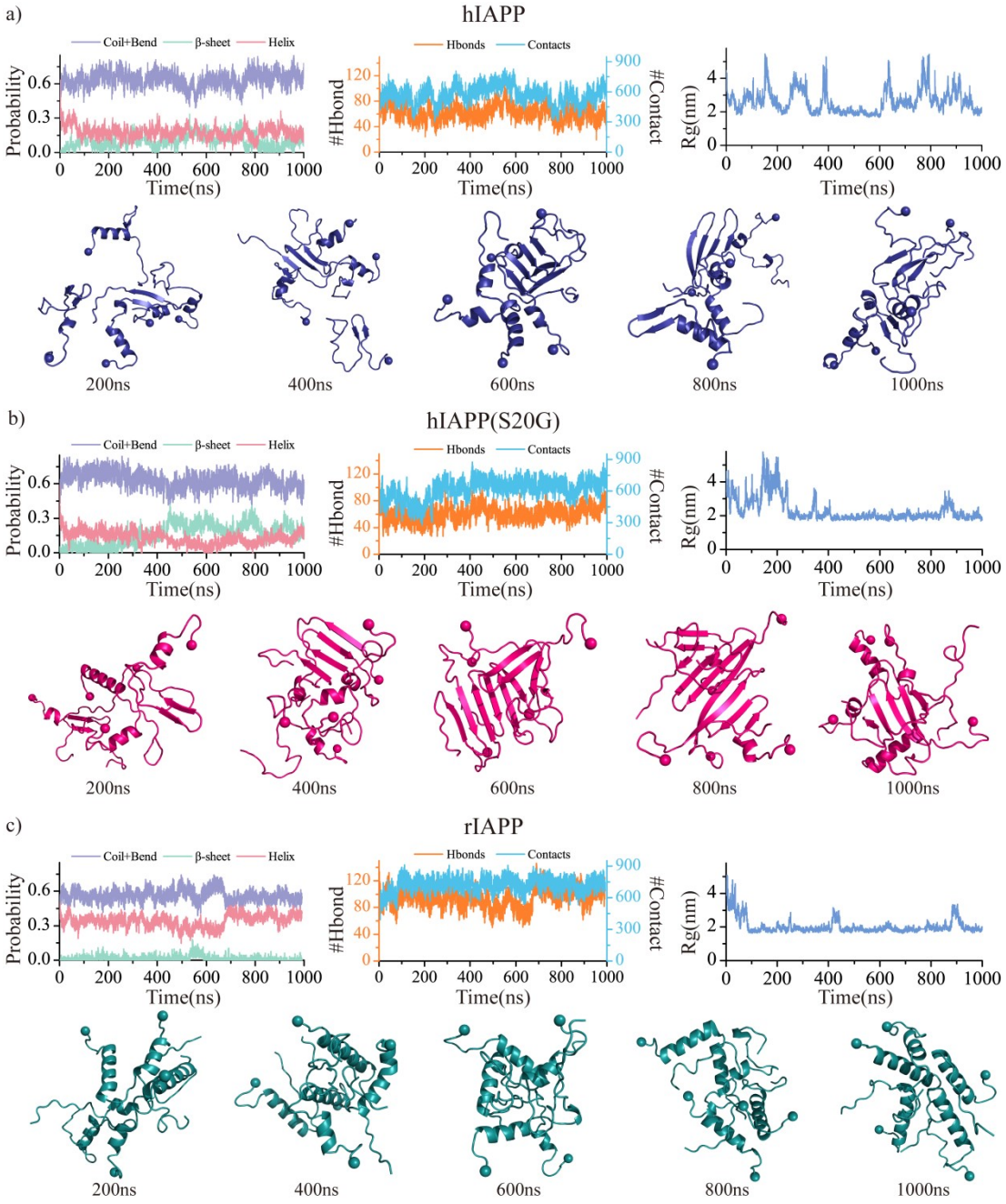

Fig. S5. Time evolution of the probability of unstructured formations (bend and random coil), helix and β-sheet, the total number of hydrogen bonds and contact, and the radius gyration for the five-peptide simulations of hIAPP a), hIAPP(S20G) b), and rIAPP c). One trajectory was randomly selected from 60 independent DMD simulation trajectories for each monomeric system. The N-terminal Cα atom is highlighted as a bead.

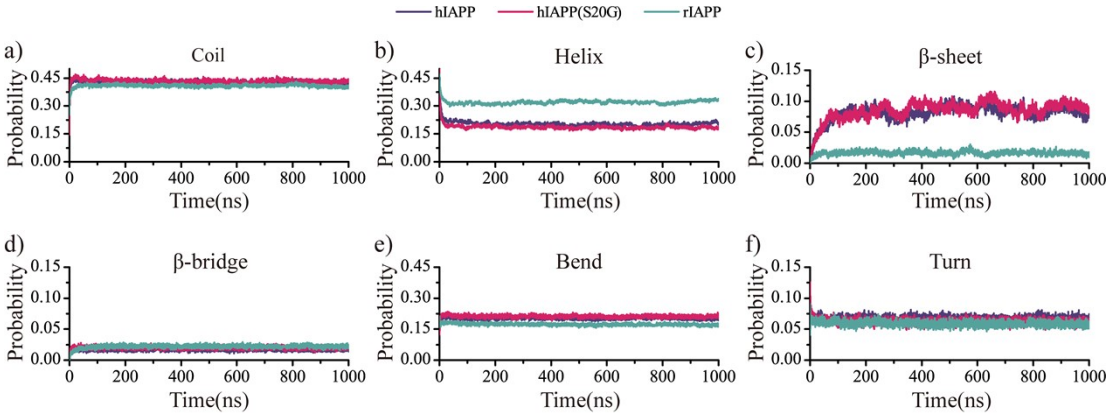

Fig. S6. Time evolution of each secondary structure (including coil, helix, β-sheet, β-bridge, bend, and turn) content averaged over 60 independent DMD simulation trajectories for each type of amylin in the five-peptide simulations.

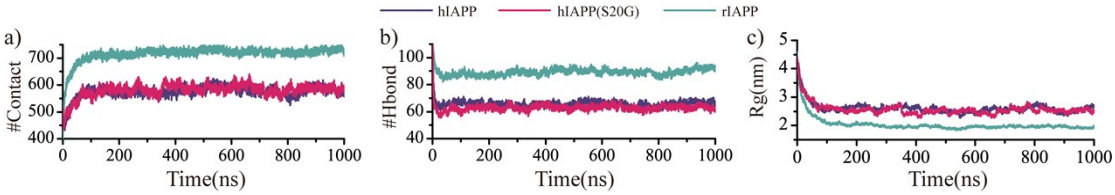

Fig. S7. Time evolution of the number of contacts, hydrogen bonds, and radius gyration (Rg) averaged over the 60 independent DMD simulations in the five-peptide simulation of hIAPP, hIAPP(S20G), and rIAPP.

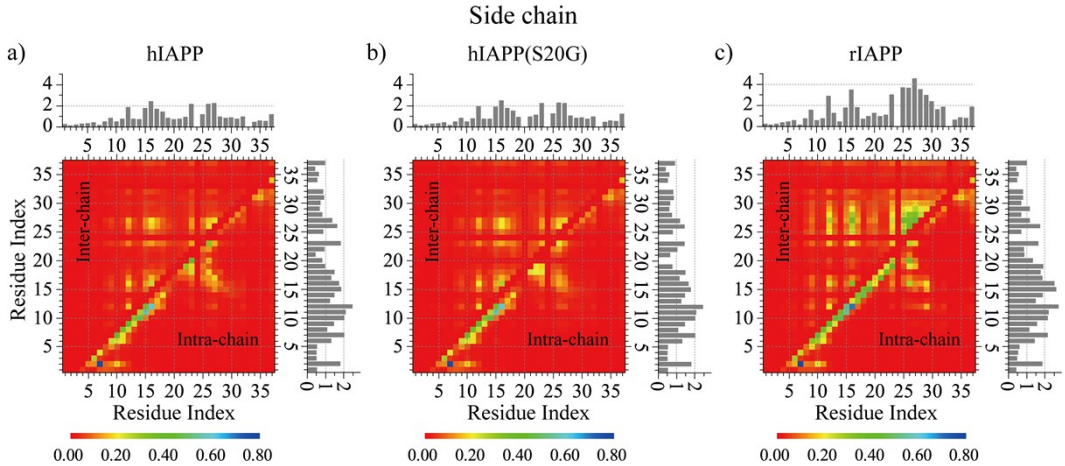

Fig. S8. The residue-pairwise contact frequency of side-chain atoms. The frequency of inter-chain (upper diagonal) and intra-chain (lower diagonal) inter-residue contact formed by side-chain atoms are calculated by averaging over the last 500 ns trajectories of all independent simulations for hIAPP a), hIAPP(S20G) b), and rIAPP c).

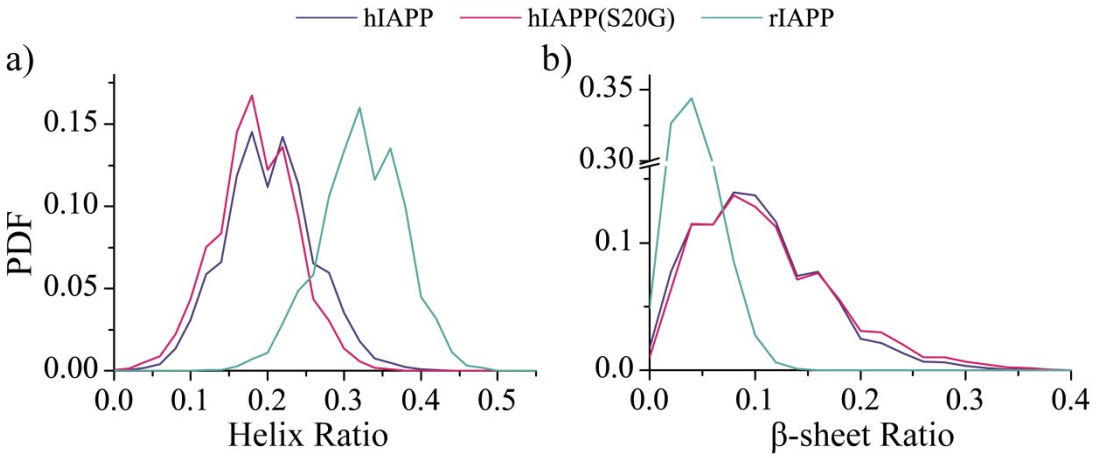

Fig. S9. Oligomeric conformational analysis. The probability distribution of helix a) and β-sheet b) content for each oligomer aggregated by hIAPP, hIAPP(S20G) and rIAPP peptides. Only the last 500 ns oligomers from sixty independent DMD simulations were used for the conformational analysis.

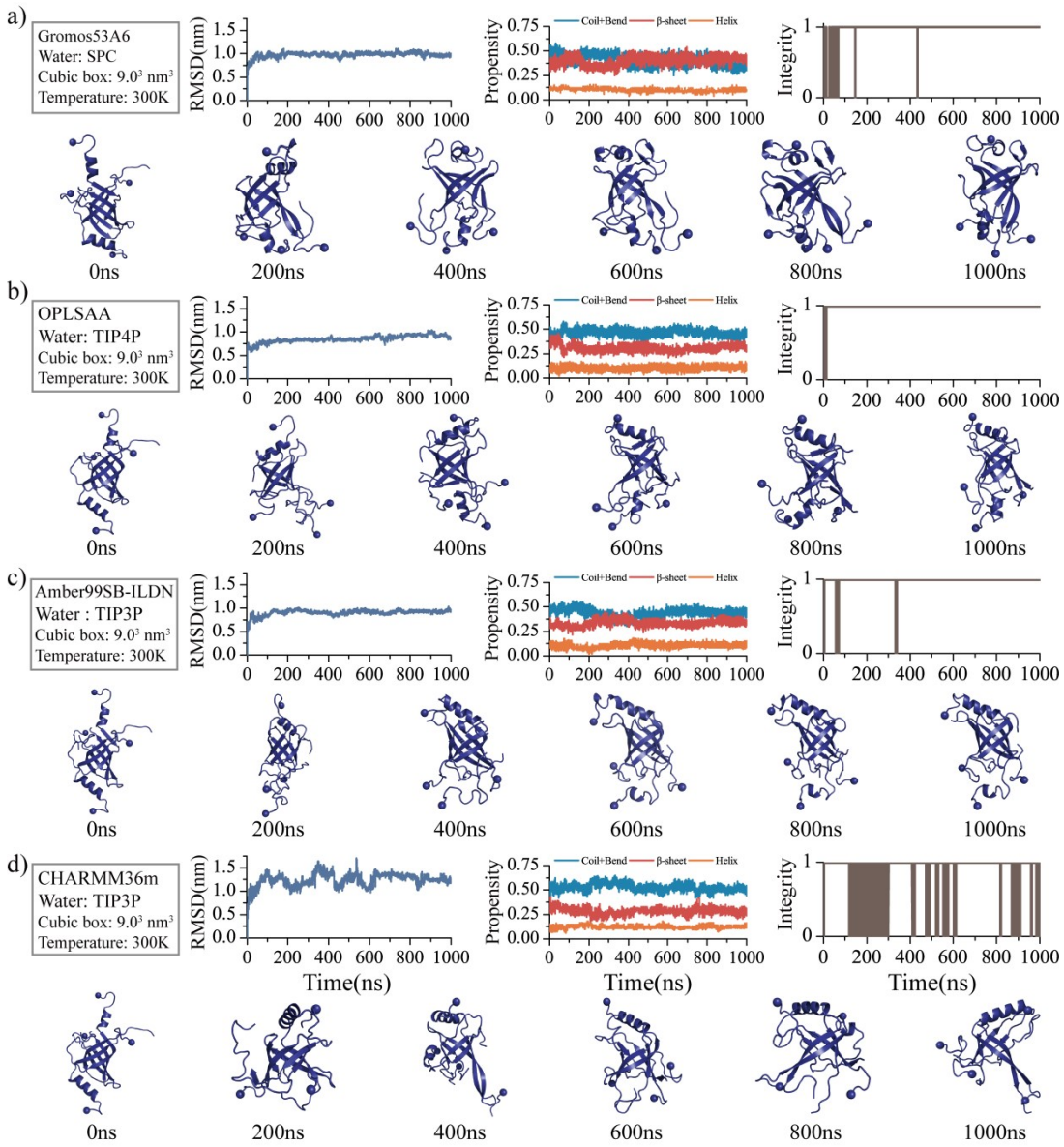

Fig. S10. The structural stability of hIAPP β-barrel formation obtained from DMD simulations is examined by all-atom standard MD simulations. The initial hIAPP β-barrel structure is randomly selected from the DMD trajectory with the most populated β-barrel formation as the initial structure for the standard all-atom MD simulations. One 1000-ns classical MD simulation with the explicit solvent model is performed using GROMOS96[1] a), OPLS-AA[2] b), AMBER99SB-ILDN[3] c), and CHARMM36m[4] d) force fields at 300K. The conformational changes are monitored by the time evolution of the root-mean-square deviation (RMSD) of backbone atoms, the secondary structure content (including random coil and bend, β-sheet, and helix), and the integrity of the β-barrel structure in each independent DMD simulation. If one oligomer has one closed cycle β-sheet layer, the integrity of the β-barrel structure will be described as 1; otherwise, the integrity of the β-barrel structure is set to 0 as a non-β-barrel structure. The snapshots along the simulation trajectory are also presented every 200 ns. Despite small variations of the exact values in the RMSD and the content of each secondary structure from simulations with different force fields, the hIAPP β-barrel structure is well dynamically conserved and undergoes open-and-close dynamics during the course of traditional MD simulations.

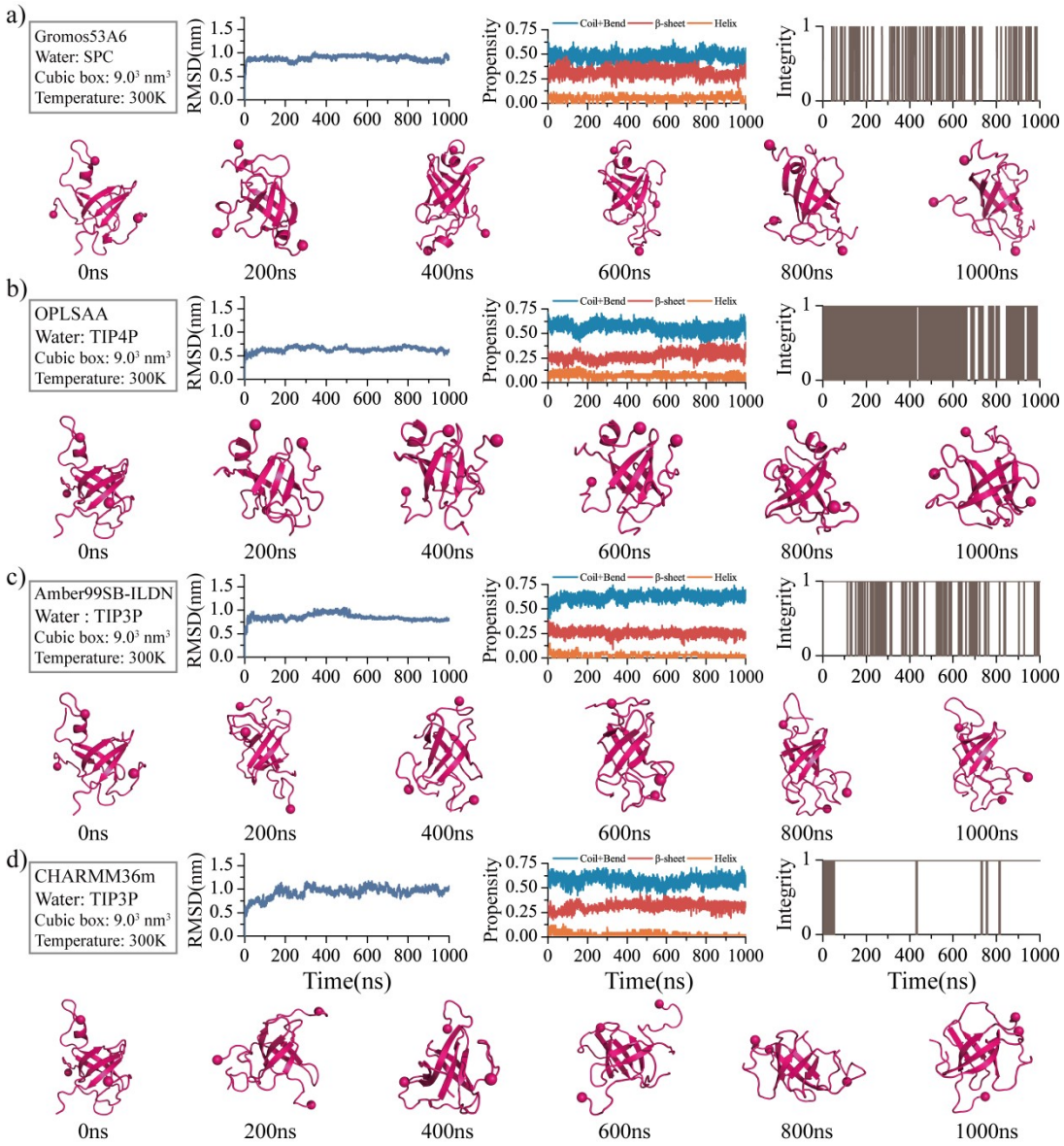

Fig. S11. The structural stability of hIAPP(S20G) β-barrel formation obtained from DMD simulations is examined by all-atom standard MD simulations. The initial hIAPP(S20G) β-barrel structure is randomly selected from the DMD trajectory with the most populated β-barrel formation as the initial structure for the standard all-atom MD simulations. One 1000-ns classical MD simulation with the explicit solvent model is performed using GROMOS96[1] a), OPLS-AA[2] b), AMBER99SB-ILDN[3] c), and CHARMM36m[4] d) force fields at 300K. The conformational changes are monitored by the time evolution of the backbone atoms' root-mean-square deviation (RMSD), the secondary structure content (including random coil+bend, β-sheet, and helix), and the integrity of the β-barrel structure in each independent DMD simulation. If one oligomer has one closed cycle β-sheet layer, the integrity of the β-barrel structure will be described as 1; otherwise, the integrity of the β-barrel structure is set to 0 as a non-β-barrel structure. The snapshots along the simulation trajectory are also presented every 200 ns. The RMSD of conformational changes is within 1.0 nm in all simulations. The exact values of each secondary structure's content are a little different in simulations with various force fields. The hIAPP(S20G) β-barrel structure is also well dynamically maintained with open-and-close dynamics during the course of traditional MD simulations.

Table S1. The correlation between the formation of β-barrel intermediates and the cytotoxicity in serials amyloid segments with contrasting cytotoxicity in prior studies and this work. The β-barrel propensity of wild-type $A\beta_{1-42}$ was stronger than the AD-protective A2T mutant but weaker than the AD-enhancing mutant of D7N and E22G[5]. The S20G substitution in hIAPP resulted in more amyloidogenic and cytotoxic than wild-type hIAPP[6, 7], and our result demonstrated the formation of the β-barrel propensity of hIAPP(S20G) was much more potent than the wild-type hIAPP.

Amyloid peptide		Barrel	Reference
Toxic	Non-toxic		
$hIAPP_{19-29}$		Yes	8
$hIAPP_{19-29}$(S20G)		Yes	8
	$hIAPP_{15-25}$	No	8
	$hIAPP_{15-25}$(S20G)	No	8
$SOD1_{28–38}$		Yes	9
	$SOD1_{28–38}$(G33W)	No	9
	$SOD1_{28–38}$(G33V)	No	9
$A\beta_{16-22}$		Yes	10, 11
$A\beta_{25-35}$		Yes	12
αB-crystalline$_{90-100}$		Yes	13
α-synuclein $_{68–78}$		Yes	14
$A\beta_{1-42}$		Yes	15, 16
$A\beta_{1-42}$(A2T)		Yes	15
$A\beta_{1-42}$(D7N)		Yes	15
$A\beta_{1-42}$(E22G)		Yes	15
$hIAPP_{1-37}$		Yes	17
$hIAPP_{1-37}$(S20G)		Yes	this study
	$rIAPP_{1-37}$	No	this study

References.

1. C. Oostenbrink, T. A. Soares, N. F. van der Vegt and W. F. van Gunsteren, *Eur Biophys J*, 2005, **34**, 273-284.
2. G. A. Kaminski, R. A. Friesner, J. Tirado-Rives and W. L. Jorgensen, *Journal of Physical Chemistry B*, 2001, **105**, 6474-6487.
3. K. Lindorff-Larsen, S. Piana, K. Palmo, P. Maragakis, J. L. Klepeis, R. O. Dror and D. E. Shaw, *Proteins*, 2010, **78**, 1950-1958.
4. J. Huang, S. Rauscher, G. Nawrocki, T. Ran, M. Feig, B. L. de Groot, H. Grubmuller and A. D. MacKerell, Jr., *Nat Methods*, 2017, **14**, 71-73.
5. P. Krotee, J. A. Rodriguez, M. R. Sawaya, D. Cascio, F. E. Reyes, D. Shi, J. Hattne, B. L. Nannenga, M. E. Oskarsson, S. Philipp, S. Griner, L. Jiang, C. G. Glabe, G. T. Westermark, T. Gonen and D. S. Eisenberg, *Elife*, 2017, **6**.
6. S. Sakagashira, H. J. Hiddinga, K. Tateishi, T. Sanke, T. Hanabusa, K. Nanjo and N. L. Eberhardt, *Am J Pathol*, 2000, **157**, 2101-2109.
7. D. T. Meier, L. Entrup, A. T. Templin, M. F. Hogan, M. Mellati, S. Zraika, R. L. Hull and S. E. Kahn, *Diabetologia*, 2016, **59**, 2166-2171.
8. Y. Sun, X. Ge, Y. Xing, B. Wang and F. Ding, *Sci Rep*, 2018, **8**, 10353.
9. Y. Sun, J. Huang, X. Duan and F. Ding, *J Chem Inf Model*, 2021, **61**, 966-975.
10. L. Xie, Y. Luo and G. Wei, *J Phys Chem B*, 2013, **117**, 10149-10160.
11. X. Ge, Y. Sun and F. Ding, *Biochim Biophys Acta Biomembr*, 2018, **1860**, 1687-1697.
12. T. D. Do, N. E. LaPointe, R. Nelson, P. Krotee, E. Y. Hayden, B. Ulrich, S. Quan, S. C. Feinstein, D. B. Teplow, D. Eisenberg, J. E. Shea and M. T. Bowers, *J Am Chem Soc*, 2016, **138**, 549-557.
13. A. Laganowsky, C. Liu, M. R. Sawaya, J. P. Whitelegge, J. Park, M. Zhao, A. Pensalfini, A. B. Soriaga, M. Landau, P. K. Teng, D. Cascio, C. Glabe and D. Eisenberg, *Science*, 2012, **335**, 1228-1231.
14. Y. Sun, A. Kakinen, C. Zhang, Y. Yang, A. Faridi, T. P. Davis, W. Cao, P. C. Ke and F. Ding, *Nanoscale*, 2019, **11**, 11933-11945.

15. Y. Sun, A. Kakinen, X. Wan, N. Moriarty, C. P. J. Hunt, Y. Li, N. Andrikopoulos, A. Nandakumar, T. P. Davis, C. L. Parish, Y. Song, P. C. Ke and F. Ding, *Nano Today*, 2021, **38**.
16. J. Wu, T. B. Blum, D. P. Farrell, F. DiMaio, J. P. Abrahams and J. Luo, *Angew Chem Int Ed Engl*, 2021, **60**, 18680-18687.
17. Y. Sun, A. Kakinen, Y. Xing, E. H. Pilkington, T. P. Davis, P. C. Ke and F. Ding, *Biochim Biophys Acta Mol Basis Dis*, 2019, **1865**, 434-444.